J Solid State Electrochem (2012) 16:481–490
DOI 10.1007/s10008-011-1356-1

ORIGINAL PAPER

Effects of complexants on $[Ni_{1/3}Co_{1/3}Mn_{1/3}]CO_3$ morphology and electrochemical performance of $LiNi_{1/3}Co_{1/3}Mn_{1/3}O_2$

Shunyi Yang · Xianyou Wang · Quanqi Chen · Xiukang Yang · Jiaojiao Li · Qiliang Wei

Received: 11 November 2010 / Revised: 18 February 2011 / Accepted: 28 February 2011 / Published online: 6 April 2011

Abstract $LiNi_{1/3}Co_{1/3}Mn_{1/3}O_2$ cathode materials for the application of lithium ion batteries were synthesized by carbonate co-precipitation routine using different ammonium salt as a complexant. The structures and morphologies of the precursor $[Ni_{1/3}Co_{1/3}Mn_{1/3}]CO_3$ and $LiNi_{1/3}Co_{1/3}Mn_{1/3}O_2$ were investigated through X-ray diffraction, scanning electron microscope, and transmission electron microscopy. The electrochemical properties of $LiNi_{1/3}Co_{1/3}Mn_{1/3}O_2$ were examined using charge/discharge cycling and cyclic voltammogram tests. The results revealed that the microscopic structures, particle size distribution, and the morphology properties of the precursor and electrochemical performance of $LiNi_{1/3}Co_{1/3}Mn_{1/3}O_2$ were primarily dependent on the complexant. Among all as-prepared $LiNi_{1/3}Co_{1/3}Mn_{1/3}O_2$ cathode materials, the sample prepared from Na_2CO_3–NH_4HCO_3 routine using NH_4HCO_3 as the complexant showed the smallest irreversible capacity of 19.5 mAh g^{-1} and highest discharge capacity of 178.4 mAh g^{-1} at the first cycle as well as stable cycling performance (98.7% of the initial capacity was retained after 50 cycles) at 0.1 C (20 mA g^{-1}) in the voltage range of 2.5–4.4 V vs. Li^+/Li. Moreover, it delivered high discharge capacity of over 135 mAh g^{-1} at 5 C (1,000 mA g^{-1}).

Keywords Lithium ion batteries · $LiNi_{1/3}Co_{1/3}Mn_{1/3}O_2$ · Carbonate co-precipitation method · Complexant · Spherical particles

S. Yang · X. Wang (✉) · Q. Chen · X. Yang · J. Li · Q. Wei
Key Laboratory of Environmentally Friendly Chemistry and Applications of Ministry of Education, School of Chemistry, Xiangtan University,
Hunan Xiangtan 411105, China
e-mail: wxianyou@yahoo.com

Introduction

In recent years, $Li[Ni_xCo_{1-2x}Mn_x]O_2(0<\times<1/2)$ has been reported as a promising cathode material for lithium ion batteries [1–3]. In particular, $LiNi_{1/3}Co_{1/3}Mn_{1/3}O_2$ (x=1/3) shows the best cell performance. The main advantages of $LiNi_{1/3}Co_{1/3}Mn_{1/3}O_2$, compared with Li–M ($M$=Co, Mn, or Ni) oxides, are its higher reversible capacity, improved thermal stability, and lowered toxicity [4–6]. Therefore, there is a great deal of interests in using $LiNi_{1/3}Co_{1/3}Mn_{1/3}O_2$ as the positive electrode material for high energy density and high power density Li-ion secondary batteries. Generally, $LiNi_{1/3}Co_{1/3}Mn_{1/3}O_2$ has mainly been prepared by solid-state reaction and hydroxide co-precipitation method. The solid-state reaction method often results in an impure and inhomogeneous product with inferior electrochemical performance [7–9]. This leads to the widespread adoption of the hydroxide co-precipitation method in which a homogeneous precursor of $[Ni_{1/3}Co_{1/3}Mn_{1/3}](OH)_2$ is prepared [10–14]. But the mixed transition metal hydroxide is unstable in hydroxide co-precipitation process; $Mn(OH)_2$ (Mn^{2+}) can easily be oxidized to MnOOH (Mn^{3+}) or MnO_2 (Mn^{4+}) upon precipitation conditions, which can decrease the homogeneity of the final product. Therefore, preparing the precursor reproducibly is very difficult [15].

Compared with solid-state and hydroxide co-precipitation methods, the carbonate co-precipitation method results in a homogeneous and phase-pure precursor of $[Ni_{1/3}Co_{1/3}Mn_{1/3}]CO_3$ in which the manganese remains as Mn^{2+}, and then it can be used for the synthesis of a more homogeneous and pure $LiNi_{1/3}Co_{1/3}Mn_{1/3}O_2$ with high electrochemical performance [4, 16–18]. During the carbonate co-precipitation process, the morphology and size of the $[Ni_{1/3}Co_{1/3}Mn_{1/3}]CO_3$ precursor were affected by operating conditions such as

reaction temperature (T), crystallization time (t), stirring speed (r), and pH of the solution [19–23]. In addition, it has been believed that the complexant is a critical factor to influence the properties of $[Ni_{1/3}Co_{1/3}Mn_{1/3}]CO_3$ precursors and $LiNi_{1/3}Co_{1/3}Mn_{1/3}O_2$ final product.

In this work, the effects of the complexants (including NH_4OH, $(NH_4)_2SO_4$, and NH_4HCO_3 as sources of NH_3 ligand) on the particle size distribution and morphology of the $[Ni_{1/3}Co_{1/3}Mn_{1/3}]CO_3$ precursor were discussed. The structure, morphology, and electrochemical performance of the as-prepared $LiNi_{1/3}Co_{1/3}Mn_{1/3}O_2$ were also studied in detail.

Experimental

Spherical $[Ni_{1/3}Co_{1/3}Mn_{1/3}]CO_3$ carbonate precursor was first synthesized by carbonate co-precipitation method. A 1.8-M mixture solution of $NiSO_4$, $CoSO_4$, and $MnSO_4$ (Ni/Mn/Co=1:1:1 M ratio) was pumped into a continuous-flow-stirred tank reactor with a 3-L capacity. At the same time, a 1.8-M aqueous solution of Na_2CO_3 and a desired amount of complexant (NH_4OH, $(NH_4)_2SO_4$, and NH_4HCO_3 solutions) with the same concentration of NH_4^+ ions were separately fed into the reactor. The mixture solution was stirred at a speed of 1,000 rpm for 12 h at 60 °C and pH=7.5 to produce the precipitation. Then, the precipitation was filtered, washed, and dried in a vacuum oven at 40 °C for several hours. Thus, the prepared powder was further dried at 110 °C to remove the adsorbed water and to obtain precursor carbonate powder $[Ni_{1/3}Co_{1/3}Mn_{1/3}]CO_3$. The $[Ni_{1/3}Co_{1/3}Mn_{1/3}]CO_3$ was fired at 500 °C for 5 h to decompose the carbonate into an oxide compound. Finally, the obtained de-carbonated oxide compound powder was mixed thoroughly with 5% excess amounts of $LiOH{\cdot}H_2O$ (molar ratio of 1.05) to compensate the calcining loss. The mixture was preheated at 500 °C for 5 h to melt the lithium salt and calcined at 900 °C for 12 h in air to obtain $LiNi_{1/3}Co_{1/3}Mn_{1/3}O_2$. The $[Ni_{1/3}Co_{1/3}Mn_{1/3}]CO_3$ prepared from Na_2CO_3–NH_4OH, Na_2CO_3–$(NH_4)_2SO_4$, and Na_2CO_3–NH_4HCO_3 systems were, respectively, denoted as precursor AH, AS, and AB, and the corresponding $LiNi_{1/3}Co_{1/3}Mn_{1/3}O_2$ were labeled as sample AH, AS, and AB, respectively.

The chemical compositions of the resulting powders were analyzed by atomic absorption spectroscopy (AAS; Vario 6 Analytik Jena AG, Jena, Germany). The phase identification of the samples was performed with a diffractometer (D/Max-3C, Rigaku, Japan) using Cu Kα radiation (λ=1.54178 Å) and a graphite monochromator at 36 kV, 20 mA. The scanning rate was 8°/min, and the scanning range of diffraction angle (2θ) was $10°\leq 2\theta \leq 80°$. In order to analyze the correlation lengths (the apparent crystallite sizes) of the $[Ni_{1/3}Co_{1/3}Mn_{1/3}]CO_3$ and $LiNi_{1/3}Co_{1/3}Mn_{1/3}O_2$ crystals in the 2D confinement, the Scherrer's equation was used:

$$D_{hkl} = \frac{K\lambda}{\beta_{hkl}\cos\theta} \quad (1)$$

Where D_{hkl} is the mean crystallite size along the (hkl) direction, K is the shape factor (the Scherrer constant, a value of 0.94 was used in this study [24]), β_{hkl} is the line breadth, and θ is the half-scattering angle. Usually, β_{hkl} is taken as the half width at half maximum of the (hkl) diffraction. The morphology of the sample was observed using scanning electron microscopy (SEM; JSM-5600LV, JEOL, Japan) and transmission electron microscopy (TEM; Tecnai G2, FEI, America). The particle size and particle size distribution were measured by Mastersizer-2000 (Malvern Instruments Ltd, England).

The electrochemical tests of $LiNi_{1/3}Co_{1/3}Mn_{1/3}O_2$ were carried out using coin cells assembled in an argon-filled glove box. In all cells, the cathode comprised a mixture of active material (80 wt.%), acetylene black (10 wt.%), graphite (5 wt.%), and polyvinylidene fluoride (5 wt.%) as binder agent, lithium was served as counter and reference electrodes, a Celgard 2400 was used as separator, and the electrolyte was a 1 M $LiPF_6$ solution in ethylene carbonate–dimethyl carbonate (1:1 v/v). Charge–discharge measurement was carried out in Neware battery test system BTS-XWJ-6.44S-00052 (Newell, Shenzhen, China) at different current densities at room temperature. Cyclic voltammogram was measured at a scan rate of 0.1 mV s^{-1} between 2.5 and 4.8 V using a CHI600A Electrochemical Analyzer (Chinstr, Shanghai, China).

Results and discussion

Usually, during the precipitation process the crystals go through two stages: the formation of crystal nuclei and their subsequent growth which includes each single-crystal nucleus development and the agglomeration of some nuclei. The above two processes determine the size and morphology of crystals. In order to get the homogeneous micron-spherical crystals $[Ni_{1/3}Co_{1/3}Mn_{1/3}]CO_3$, NH_3 ligand was introduced to carbonate co-precipitation reaction system to keep the balance of crystal nucleation rate and crystal growth rate [18–21]. In this work, NH_4OH, $(NH_4)_2SO_4$, and NH_4HCO_3 were separately used as complexants to provide the NH_3 ligand; the mechanism of formation of the crystal nucleus

$[Ni_{1/3}Co_{1/3}Mn_{1/3}]CO_3$ can be explained according to the following two-step process [18]:

$$1/3Ni^{2+}(aq.) + 1/3Co^{2+}(aq.) + 1/3Mn^{2+}(aq.) + nNH_3 \cdot H_2O(aq.) \rightarrow \left[Ni_{1/3}Co_{1/3}Mn_{1/3}(NH_3)_n\right]^{2+}(aq.) + nH_2O \quad (2)$$

$$\left[Ni_{1/3}Co_{1/3}Mn_{1/3}(NH_3)_n\right]^{2+}(aq.) + CO_3^{2-} + nH_2O \rightarrow \left[Ni_{1/3}Co_{1/3}Mn_{1/3}\right]CO_3(s.) + nNH_3 \cdot H_2O(aq.) \quad (3)$$

This mechanism suggests the formation of an intermediary, ammoniacal-mixed transition metal ligand, during the first step. The ligand becomes unstable in the presence of an increasing concentration of carbonate, and replacement of the ammoniacal groups takes place during the second step. The uniformity was attributed to the action of the complexant, which basically prevents the phase separation and leads to the formation of homogeneous and uniform carbonate particles. In the previous reports [25, 26], the morphology and homogeneity of the carbonate powders prepared in the absence of complexant were significantly inferior. While in this work, homogeneous and spherical $[Ni_{1/3}Co_{1/3}Mn_{1/3}]CO_3$ was successfully synthesized by carbonate precipitation method using Na_2CO_3 precipitant and different complexants (NH_4OH, $(NH_4)_2SO_4$, and NH_4HCO_3) as shown in Fig. 1. The microstructures of $[Ni_{1/3}Co_{1/3}Mn_{1/3}]CO_3$ particles are strongly influenced by the complexants. SEM images of precursors presented in Fig. 1 show that all $[Ni_{1/3}Co_{1/3}Mn_{1/3}]CO_3$ precursors are spherical and homogeneous. However, precursor AH prepared by Na_2CO_3–NH_4OH system was more round and smoother than precursors AS and AB, suggesting that the different complexants are responsible for the difference of precursors in shape. The particle size and particle size distribution of $[Ni_{1/3}Co_{1/3}Mn_{1/3}]CO_3$ precursors are shown in Fig. 2. The average particle size of the precursor AH, precursor AS and precursor AB is 19.54, 19.89, and 16.87 μm, respectively, which is consistent with the SEM observations. Compared with precursors AH and AS, precursor AB prepared by Na_2CO_3–NH_4HCO_3 system has a much more narrow size distribution (diameter at 10% is 12.54 μm and the diameter at 90% is 22.93 μm), indicating that in Na_2CO_3–NH_4HCO_3 system, a good pH buffer solution can keep the balance of crystal nucleation rate and crystal growth rate, which is much better than in the other two precipitator-complexant systems.

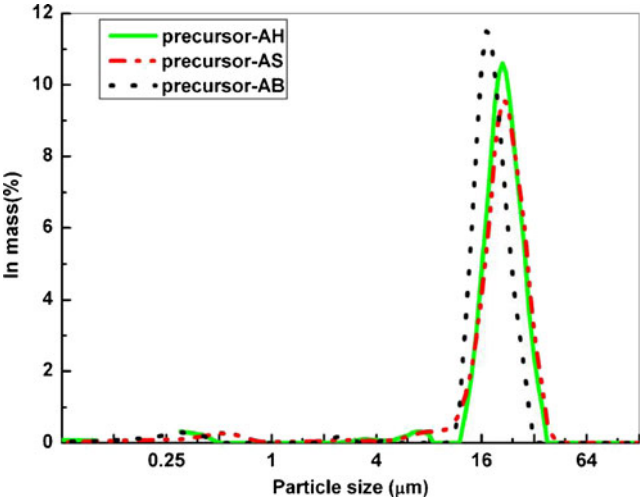

Fig. 2 Particle size distribution of the precursors $[Ni_{1/3}Co_{1/3}Mn_{1/3}]CO_3$

Figure 3 shows the X-ray diffraction (XRD) patterns of the $[Ni_{1/3}Co_{1/3}Mn_{1/3}]CO_3$ powders prepared from Na_2CO_3–NH_4OH, Na_2CO_3–$(NH_4)_2SO_4$, and Na_2CO_3–NH_4HCO_3 systems. The co-precipitated carbonate is single phased and has a typical structure corresponding to those of $NiCO_3$, $CoCO_3$, and $MnCO_3$, all of which have divalent transition metals in their formal charge. This structure was indexed to a hexagonal structure with a space group of $R\bar{3}c$[18]. The diffraction peaks were quite broad due to the

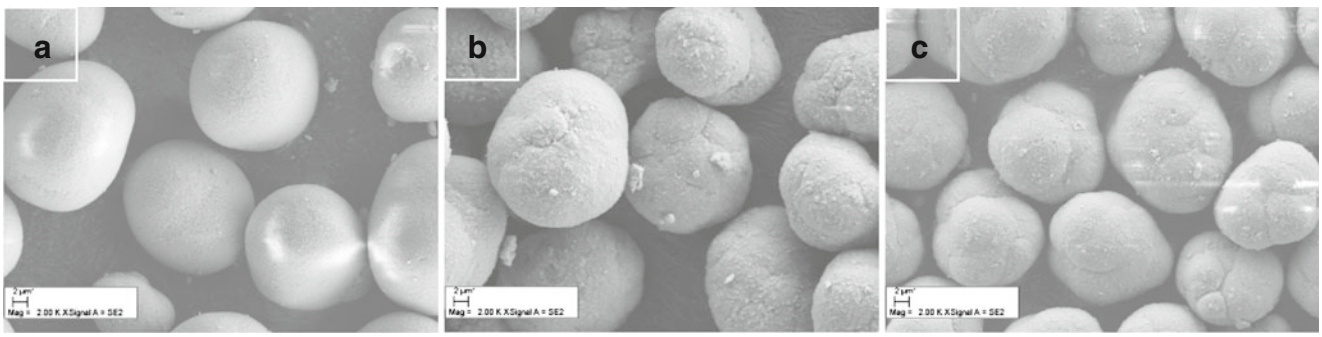

Fig. 1 Scanning electron micrographs of the precursors $[Ni_{1/3}Co_{1/3}Mn_{1/3}]CO_3$ **a** precursor AH, **b** precursor AS, and **c** precursor AB

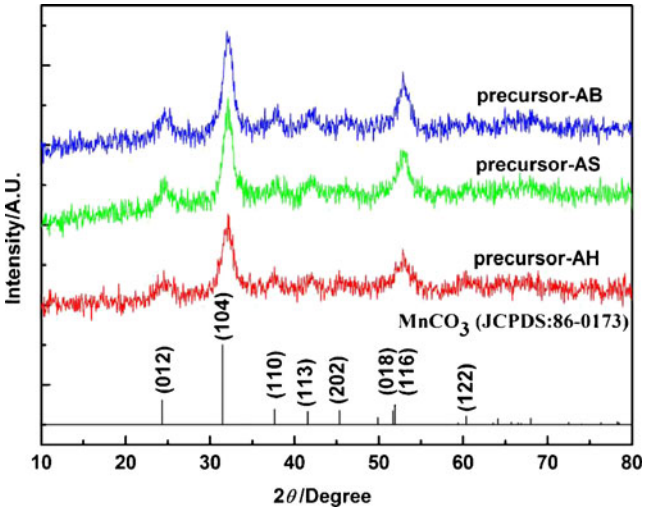

Fig. 3 XRD patterns of the $[Ni_{1/3}Co_{1/3}Mn_{1/3}]CO_3$ precursors and pure $MnCO_3$ (JCPDS:86–0173)

small particle size. According to the XRD patterns, the lattice parameters of *a*, *c*, and *V* were calculated by Bragg's equation and the D_{104} (the mean crystallite size along the (104) direction) was analyzed using Scherrer's equation; the results were listed in Table 1. The apparent mean crystallite sizes D_{104} of $[Ni_{1/3}Co_{1/3}Mn_{1/3}]CO_3$ powders calculated using Scherrer's equation are around 7–10 nm, indicating that all the micron-spherical $[Ni_{1/3}Co_{1/3}Mn_{1/3}]CO_3$ particles are composed of nano-sized primary particles. From the TEM images of precursor $[Ni_{1/3}Co_{1/3}Mn_{1/3}]CO_3$ (as seen in Fig. 4), it can be seen that the size of the primary particles are around 5–15 nm; these results are in good agreement with the calculated values.

Figure 5 illustrates the XRD patterns of all $Li[Mn_{1/3}Ni_{1/3}Co_{1/3}]O_2$ materials prepared by Na_2CO_3–NH_4OH, Na_2CO_3–$(NH_4)_2SO_4$, and Na_2CO_3–NH_4HCO_3, respectively. All XRD patterns can be indexed on the basis of the α-$NaFeO_2$ structure (space group: 166, $R\bar{3}m$). The observed peak splitting at (006)/(102) and (108)/(110), and the corresponding XRD patterns are magnified in the inset of Fig. 5. The peaks are clearly split, indicating the formation of a well-ordered α-$NaFeO_2$-type layered structure [27]. In the layered structure, Li^+, transition metal ions (Ni, Co, and Mn), and oxygen ion are situated in 3a, 3b, and 6c sites, respectively. Since the ionic radii of Li^+ (0.76 Å) and Ni^{2+} (0.69 Å) ions are similar, a partial disordering among the 3a and 3b sites is expected and termed as "cation mixing" [28]. It has been established that the cation mixing deteriorates the electrochemical performance of the layered oxide materials. Lattice parameters of the samples were summarized in Table 2. It is well known that the *c*/3*a* ratio of the lattice constants is a direct measure of deviation of the lattice from a perfect cubic closed-packed lattice. A pure layered lattice without transition metal in the lithium layer has a *c*/3*a* ratio of 1.672, 1.639, and 1.648 for $LiTiS_2$, $LiNiO_2$, and $LiNi_{0.5}Mn_{0.5}O_2$, respectively. The $LiMn_{1/3}Ni_{1/3}Co_{1/3}O_2$ materials synthesized by NH_4OH, $(NH_4)_2SO_4$, and NH_4HCO_3 have a *c*/3*a* ratio of 1.657, 1.656, and 1.657, respectively, implying that the material has a more ideal ccp lattice than the previously synthesized materials [28, 29]. According to Dahn's report [30], the r_I-factor defined by $(I_{006}+I_{102})/I_{101}$ is an indicator of the hexagonal ordering, the lower the r_I, the better the hexagonal ordering. Sample AB has the lowest r_I, which indicates better hexagonal ordering of its lattice than that of the samples AH and AS. In addition, the ratio of I_{003}/I_{104} is also a parameter to characterize the cation mixing and the decrease of this ratio indicates the increase of the structural deviation from hexagonal to cubic symmetry. It was reported that the undesirable cation mixing would appear when the ratio of I_{003}/I_{104} is smaller than 1.2, but the ratios of I_{003}/I_{104} for the samples AH, AS, and AB are 1.497, 1.508, and 1.548, respectively, which are larger than those reported by Li et al. [7], Shaju et al. [11], and Cho et al. [25], suggesting less cation mixing in all $LiNi_{1/3}Mn_{1/3}Co_{1/3}O_2$ samples prepared by our different carbonate precipitator-complexant systems [31]. From the above analysis, it is concluded that the sample AB prepared by Na_2CO_3–NH_4HCO_3 system displays a better structural integrity (lower r_I and higher ratio of I_{003}/I_{104}) than the sample AH, sample AS, and other materials reported in references [7, 11, 25].

The chemical compositions of the resulting powders were analyzed by atomic absorption spectroscopy; the results were listed in Table 2. The AAS analysis identified that the element ratios of Li/Ni/Mn/Co for the samples AH, AS, and AB are 1.011:0.336:0.330:0.334, 1.006:0.341:0.326:0.333, and 1.008:0.335:0.330:0.335, respectively, the element ratio of Ni/Mn/Co is close to 1:1:1, and the molar ratio of Li/M (M=Ni, Co, and Mn) is

Table 1 Lattice parameters of the spherical precursors $[Ni_{1/3}Co_{1/3}Mn_{1/3}]CO_3$

Precursor	Lattice parameters			
	a-Axis (Å)	*c*-Axis (Å)	Unit volume $(Å)^3$	D_{104} (nm)
AH	4.79110	15.01674	298.514	8.907
AS	4.82572	14.88315	300.149	9.148
AB	4.75644	15.15505	296.920	7.753

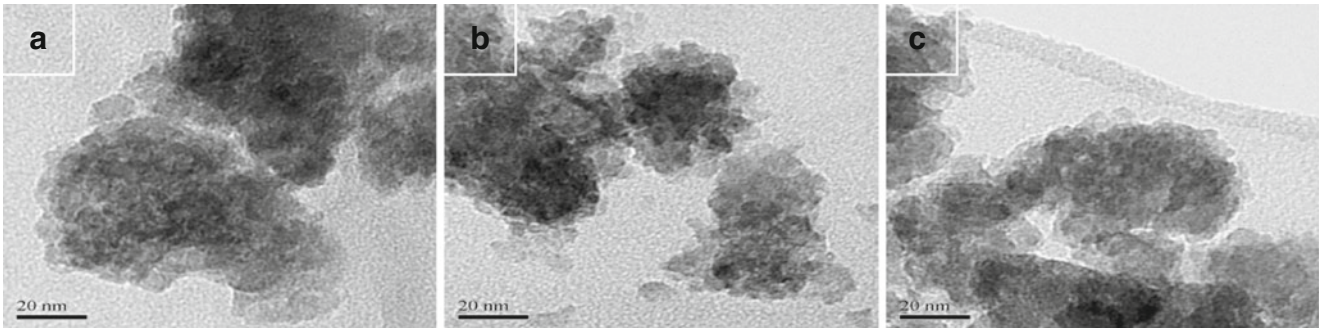

Fig. 4 TEM images of the precursor $[Ni_{1/3}Co_{1/3}Mn_{1/3}]CO_3$ **a** precursor AH, **b** precursor AS, and **c** precursor AB

also approaching 1:1, which are almost the same as the values we designed. Therefore, we could successfully prepare $Li[Mn_{1/3}Ni_{1/3}Co_{1/3}]O_2$ by carbonate co-precipitation routine.

Figure 6 shows the scanning electron micrographs of the $LiMn_{1/3}Ni_{1/3}Co_{1/3}O_2$ materials synthesized from different precipitator-complexant systems. It can be seen that the secondary particle of the prepared $LiNi_{1/3}Co_{1/3}Mn_{1/3}O_2$ has the same shape and size as those of the precursors $[Ni_{1/3}Co_{1/3}Mn_{1/3}]CO_3$ even after the precursor was re-crystallized with lithium salt during high-temperature calcination. Each of the spherical particles is made up of a large number of nano-sized primary grains as shown in Fig. 6a–c. From Scherrer's equation, the mean crystallite sizes was evaluated to be about 70–90 nm as shown in Table 2. From Fig. 6d–f, it can also be seen clearly that the primary grains of the sample AB stacked more closely than those of the samples AH and AS, close contact between the primary grains will likely improve interparticle lithium ion movement, thereby enhancing the rate capability of the material.

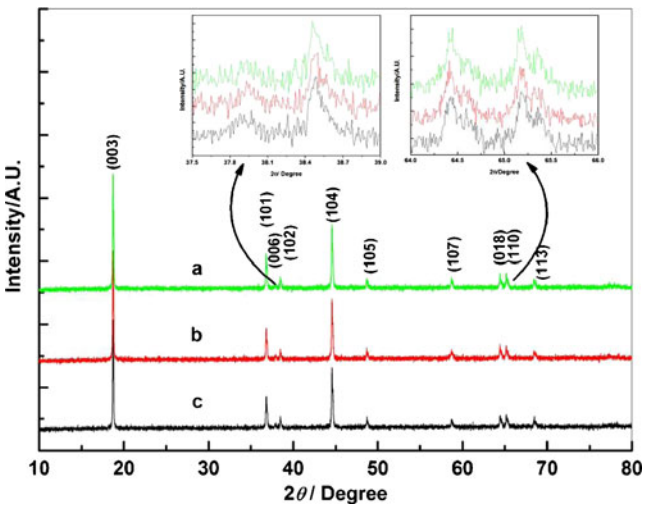

Fig. 5 XRD patterns of the prepared $LiNi_{1/3}Co_{1/3}Mn_{1/3}O_2$ **a** sample AH, **b** sample AS, and **c** sample AB

Normally, the crystal structure and morphology are two main factors which affect the electrochemical performance of the materials. Galvanostatic charge/discharge experiments of the synthesized $LiMn_{1/3}Ni_{1/3}Co_{1/3}O_2$ materials have been performed at a current density of 20 and 100 mA g^{-1} in the voltage range of 2.5–4.4 V vs. Li^+/Li. The charge/discharge curves of the $LiNi_{1/3}Co_{1/3}Mn_{1/3}O_2$ samples are presented in Figs. 7 and 8. It can be seen that the first cycle of $LiNi_{1/3}Co_{1/3}Mn_{1/3}O_2$ electrodes differs notably from successive cycles and shows more irreversible capacity loss. This might be attributed to the formation of a solid electrolyte interface on the surface of the electrode and insufficient soaking of the electrode material during the first cycle [32]. The first charge/discharge specific capacities are 198.9/174, 197.3/171.4, 197.9/178.4 mAh g^{-1} with a ratio of irreversible capacity loss of 12.52%, 13.13%, and 9.85% for the samples AH, AS, and AB, respectively, suggesting that the sample AB prepared by NH_4HCO_3 complexant exhibits the highest discharge capacity and coulombic efficiency among all prepared samples. Furthermore, the sample AB exhibits a little smaller IR drop between charge and discharge in the whole voltage range in Fig. 8, compared with those at the samples AH and AS, the cell exhibits very stable cyclability, the capacity retention after 50 cycles reaches 98.70%. Figure 9 depicts the cycle performance of the synthesized $LiNi_{1/3}Co_{1/3}Mn_{1/3}O_2$ materials at 100 mA g^{-1} current rates between 2.5 and 4.4 V. It can be seen that the samples AH, AS, and AB exhibit the initial discharge capacities of 164.8, 161.9, and 171.8 mAh g^{-1}, respectively. The capacity retention ratios of the samples AH, AS, and AB are 91.23%, 88.26%, and 93.68% after 100 cycles, respectively, the sample AB synthesized from Na_2CO_3–NH_4HCO_3 system appears to exhibit the most impressive electrochemical performance. The best results reported by Shaju et al. [11] for Layered Li $[Ni_{1/3}Co_{1/3}Mn_{1/3}]O_2$ prepared by mixed hydroxide method do not exceed 160 mAh g^{-1} at a specific current of 30 mA g^{-1} in the range of 2.5 and 4.4 V, and the retained capacity after 40 cycles was only 143 mAh g^{-1}. In other

Table 2 Chemical analysis, calculated structure parameters for $LiNi_{1/3}Co_{1/3}Mn_{1/3}O_2$ compounds

Sample	Composition	Lattice parameters			$c/3a$	$(I_{006}+I_{102})/I_{101}$	I_{003}/I_{104}	D_{003} (nm)
		a-Axis (Å)	c-Axis (Å)	Unit volume (Å)^3				
AH	$Li_{1.011}$ $Ni_{0.336}Mn_{0.330}Co_{0.334}O_2$	2.86018	14.21407	100.698	1.657	0.489	1.497	76.32
AS	$Li_{1.006}$ $Ni_{0.341}Mn_{0.326}Co_{0.333}O_2$	2.86126	14.20824	100.733	1.656	0.516	1.508	82.48
AB	$Li_{1.008}$ $Ni_{0.335}Mn_{0.330}Co_{0.335}O_2$	2.85944	14.21607	100.660	1.657	0.474	1.548	76.14
Literature [7]	–	2.852	14.208	100.09	–	–	1.25	–
Literature [11]	–	2.864	14.233	101.102	–	–	0.8	–
Literature [25]	–	2.8604(6)	14.2453 (29)	100.9353	–	–	1.45	–

respects, attractive properties have been recently reported with high tap density of $Li[Ni_{1/3}Co_{1/3}Mn_{1/3}]O_2$ synthesized from uniform co-precipitated spherical metal hydroxide $[Ni_{1/3}Co_{1/3}Mn_{1/3}](OH)_2$, the initial discharge capacity of 166.99 mAh g^{-1} was obtained between 3 and 4.3 V at a current density of 16 mA g^{-1}, and the capacity retention after 30 cycles was 93% [10].

In order to evaluate the effect of complexant on the rate capability of $LiNi_{1/3}Co_{1/3}Mn_{1/3}O_2$, the cells were charged galvanostatically with a 0.2 C (40 mA g^{-1}) rate before each

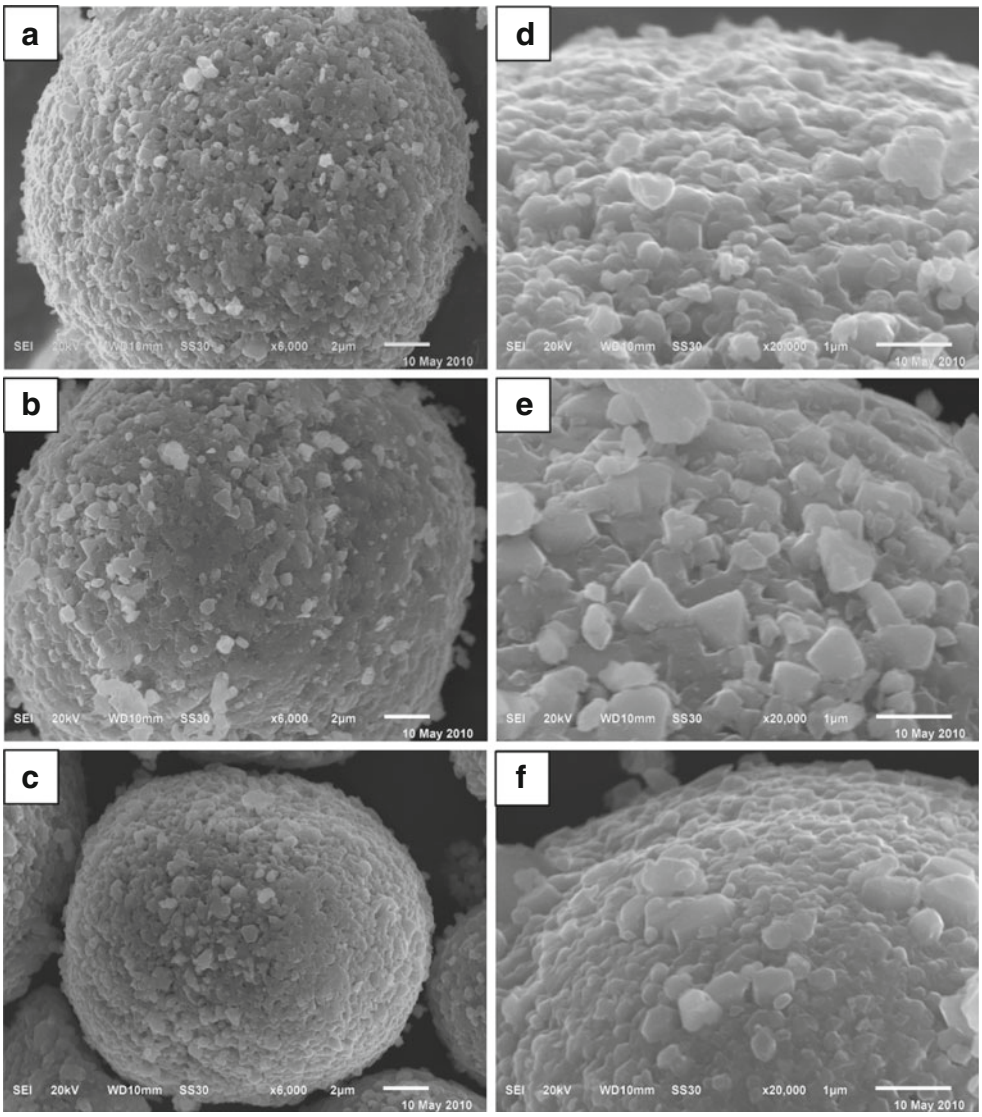

Fig. 6 SEM images of the prepared $LiNi_{1/3}Co_{1/3}Mn_{1/3}O_2$ **a**, **d** sample AH, **b**, **e** sample AS, and **c**, **f** sample AB at different magnifications

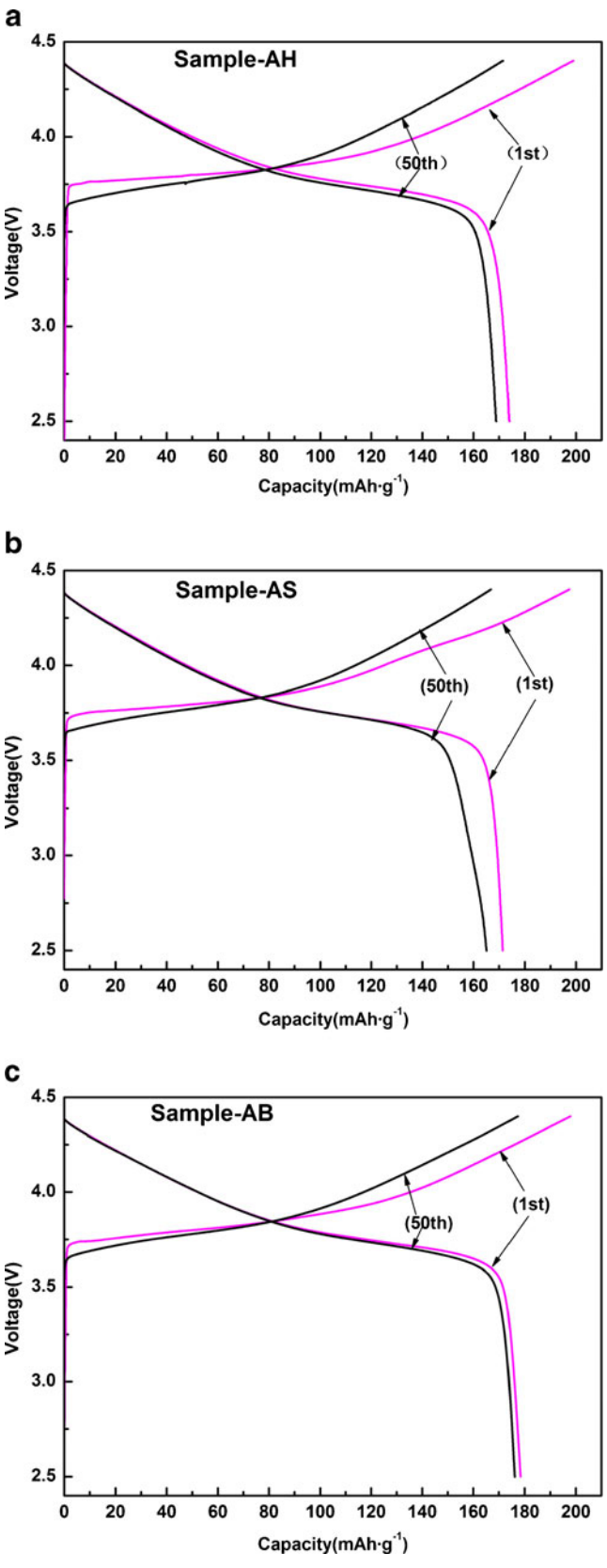

Fig. 7 First and 50th charge–discharge curves of $LiNi_{1/3}Co_{1/3}Mn_{1/3}O_2$ cathode **a** sample AH, **b** sample AS, and **c** sample AB at a current density of 20 mA g^{-1} between 2.5 and 4.4 V

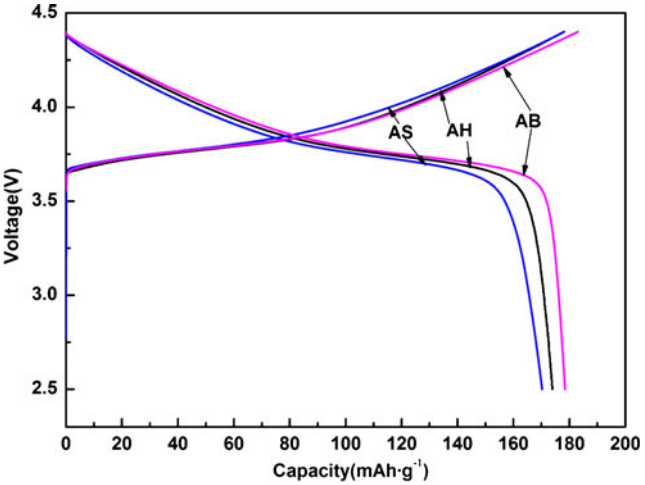

Fig. 8 The second charge–discharge curves for $LiNi_{1/3}Co_{1/3}Mn_{1/3}O_2$ the samples at a current density of 20 mA g^{-1} between 2.5 and 4.4 V

discharge testing, then discharged at different C rates from 0.2 to 5 C stepwise, and finally returned to 0.2 C. The discharge curves of $Li/LiNi_{1/3}Co_{1/3}Mn_{1/3}O_2$ cells at various current densities (40–1,000 mA g^{-1}) are shown in Fig. 10, and the corresponding cycling performance are shown in Fig. 11. The discharge capacity and average discharging voltage of the sample AH prepared from Na_2CO_3–NH_4OH system decreased with increasing current density. The capacity reached 91.9%, 83.3%, and 71.2% at 1, 2, and 5 C, respectively, compared with the specific capacity of 169.6 mA g^{-1} at 0.2 C. At the same time, the discharge capacity of the sample AS prepared from Na_2CO_3–$(NH_4)_2SO_4$ system decreased more quickly than the sample AH at high currents, only 80% and 60.2% at 2 and 5 C, respectively, remained when compared with the specific

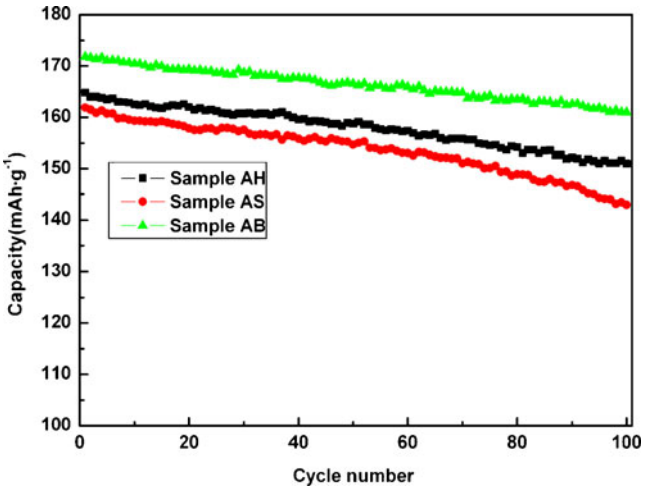

Fig. 9 Cycling performance of the prepared $LiNi_{1/3}Co_{1/3}Mn_{1/3}O_2$ sample AH (*squares*), sample AS (*circles*), and sample AB (*triangles*) at a current density of 100 mA g^{-1} between 2.5 and 4.4 V

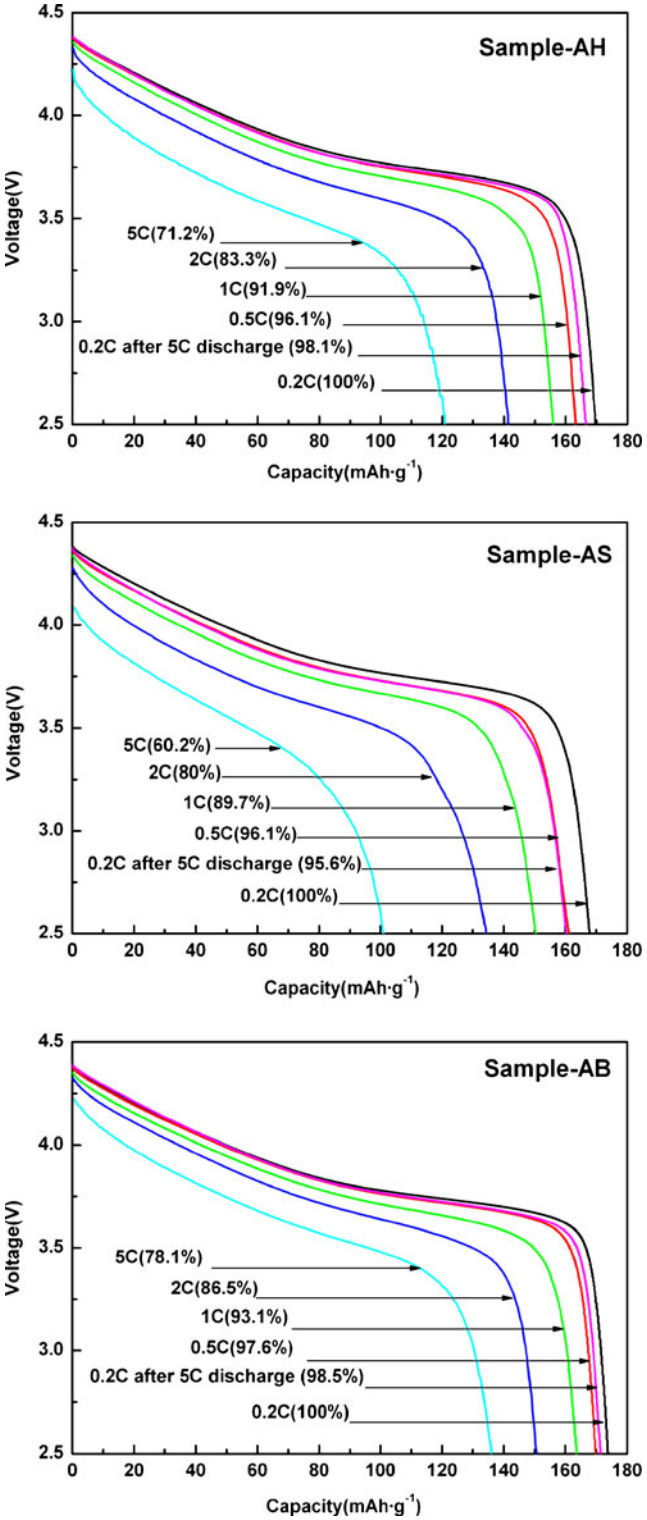

Fig. 10 Discharge curves of Li/$LiNi_{1/3}Co_{1/3}Mn_{1/3}O_2$ cell at various current densities between 2.5 and 4.4 V

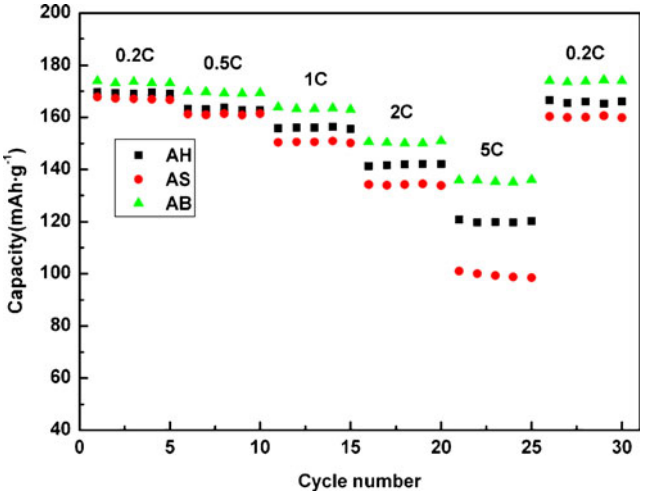

Fig. 11 Cycle performance of Li/$LiNi_{1/3}Co_{1/3}Mn_{1/3}O_2$ cell at various current densities between 2.5 and 4.4 V

capacity of 167.7 mA g^{-1} at 0.2 C. As shown in Fig. 10c, the capacity of the sample AB prepared from Na_2CO_3–NH_4HCO_3 system decreases less than that of the first two samples when the discharging current is increased from 0.2 to 5 C. It could be found that the sample AB delivers a discharge capacity of 169.9 mAh g^{-1} at 0.5 C (the capacity retention rate is about 97.6% as that of 0.2 C), 163.8 mAh g^{-1} at 1 C (the capacity retention rate is about 93.1% as that of 0.2 C), and 150.6 mAh g^{-1} at 2 C (the capacity retention rate is about 86.5% as that of 0.2 C). Even at 5 C (1,000 mA g^{-1}), the capacity of the sample AB is still as high as 135 mA g^{-1} and the capacity retention rate is about 78.1% as that of 0.2 C. Obviously, it is clear that the sample AB retains a high percentage of discharge capacity at high charge/discharge rate during cycling process, and its capacity could be recovered quickly after the high-rate discharging process (98.5% capacity was retained when compared with the first specific capacity of 174 mA g^{-1} at 0.2 C). This excellent capacity retention at a high current density is mainly attributed to the lessened extent of cationic mixing and good packing properties of the secondary particles.

$LiNi_{1/3}Co_{1/3}Mn_{1/3}O_2$ is only partially de-intercalated and intercalated when cells are charged and discharged in the voltage range of 2.5–4.4 V. Higher discharge capacities can be obtained when the voltage range is broadened, but more rapid capacity fading will be brought. To illustrate these phenomena and show the differences of the three samples operated in broader voltage, the voltage range of 2.5–4.6 V is adopted. Here, 4.6 V is chosen as the upper limit because the critical upper limit of $LiNiO_2$ and $LiCoO_2$ is 4.6 V [33]. Figure 12 shows the cycling performance of the samples AH, AS, and AB at a current density of 100 mA g^{-1} between the voltage range of 2.5 and 4.6 V. It is noticed that the initial discharge capacities for the three samples are remarkably increased. However, their speed of capacity fading also increases. The initial discharge capacities of the samples AH, AS, and AB reach 185.1, 178.3, and 193.4 mA g^{-1}, respectively; however, the capacity retention

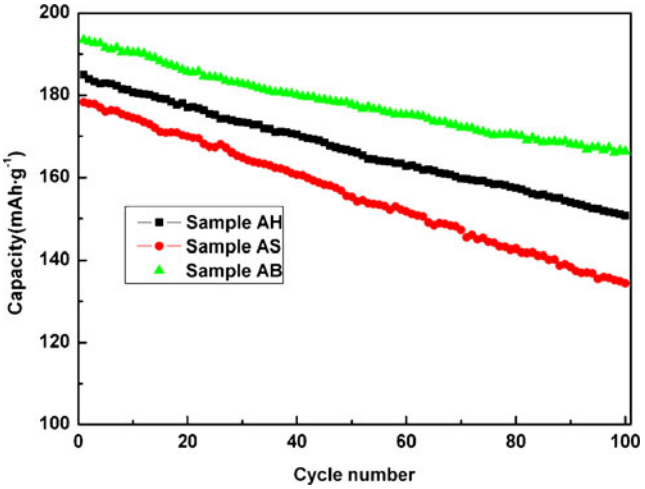

Fig. 12 Cycling performance of the prepared $LiNi_{1/3}Co_{1/3}Mn_{1/3}O_2$ sample AH (*squares*), sample AS (*circles*), and sample AB (*triangles*) at a current density of 100 mA g^{-1} between voltage range 2.5 and 4.6 V

after 100 cycles are only 81.48%, 75.37%, and 85.97%. These phenomena indicate that the different charge/discharge voltage range may have different influence on the electrochemical performance of electrode material, which correspond to research results reported by Shaju et al. [11] and Ren et al. [19].

Cyclic voltammogram was carried out to monitor the electrochemical reactions during charge/discharge process in the voltage range of 2.5–4.8 V at a scan rate of 0.1 mV s^{-1}; the first cycle curves of voltammogram for the samples AH, AS, and AB are shown in Fig. 13. It can be seen that all the three samples show the two major anodic peaks at 3.8–4.0 V and 4.5–4.7 V, whereas the corresponding major cathodic peak is at 3.5–3.7 V and 4.4–4.6 V. The redox processes of the first range roughly correspond to the expected value for Ni^{2+}/Ni^{4+} reaction, and the latter redox range can be conclusively assigned to the Co^{3+}/Co^{4+} couple. This is a quite unusual value for the Co^{3+}/Co^{4+} redox couple in a layered compound, because in similar layer-structured compounds $LiCoO_2$, the Co^{3+}/Co^{4+} couple usually appears at about 4 V and shows better reversibility [34, 35]. However, in the layered compound $Li(Mn_{1-x}Co_x)O_2$ and $Li(Ni_{1-x-y}Co_xMn_y)O_2$, the Co^{3+}/Co^{4+} couple appears at 4.4–4.6 V. This unusually high value for the redox couple could have possibly been responsible for the compounds to undergo structural transformation more easily, exhibiting the associated capacity fading during cycling in the upper voltage range near 4.6 V [36, 37]. In addition, it also can be noticed that the sample AB displays the sharper redox peak and smaller peak potential differences (ΔE) between oxidation and reduction peaks positions than the samples AH and AS. This suggests that the better reversibility of Li de-intercalation processes occur in the cell of the sample AB, which in turn, ensures a reduced capacity fade during battery cycling process.

From the above electrochemical charge/discharge, rate capability and cyclic voltammogram tests, we conclude that, of the three complexants tested herein, NH_4HCO_3 corresponds to the best complexant for preparation of $[Ni_{1/3}Co_{1/3}Mn_{1/3}]CO_3$ as the precursor of $LiNi_{1/3}Co_{1/3}Mn_{1/3}O_2$ cathode material with excellent performance. Compared with the layered $Li[Ni_{1/3}Mn_{1/3}Co_{1/3}]O_2$ prepared by carbonate co-precipitation method without using complexants reported by Cho [25], the sample AB prepared from Na_2CO_3–NH_4HCO_3 system not only shows a better structural integrity (higher ratio of I_{003}/I_{104}) but also some improvement on electrochemical performance (higher initial discharge capacity and better capacity retention).

Conclusions

Layered $LiNi_{1/3}Co_{1/3}Mn_{1/3}O_2$ cathode materials were prepared by carbonate co-precipitation methods using Na_2CO_3–NH_4OH, Na_2CO_3–$(NH_4)_2SO_4$, and Na_2CO_3–NH_4HCO_3 precipitator-complexant systems, respectively. The XRD patterns and SEM images show that different complexants result in the differences in morphology and structure of $LiNi_{1/3}Co_{1/3}Mn_{1/3}O_2$. The $LiNi_{1/3}Co_{1/3}Mn_{1/3}O_2$ prepared from Na_2CO_3–NH_4HCO_3 routine using NH_4HCO_3 as complexant has the highest capacity, best cycle performance, and excellent rate capability. The initial discharge capacity reaches 178.4 mA g^{-1}, and the capacity retention after 50 cycles is 98.7% at a current of 20 mA g^{-1} in the voltage range of 2.5–4.4 V. When the discharging current is increased from 0.2 to 5 C, it delivers a discharge capacity of 174 (0.2 C), 169.9 (0.5 C), 163.8 (1 C), 150.6

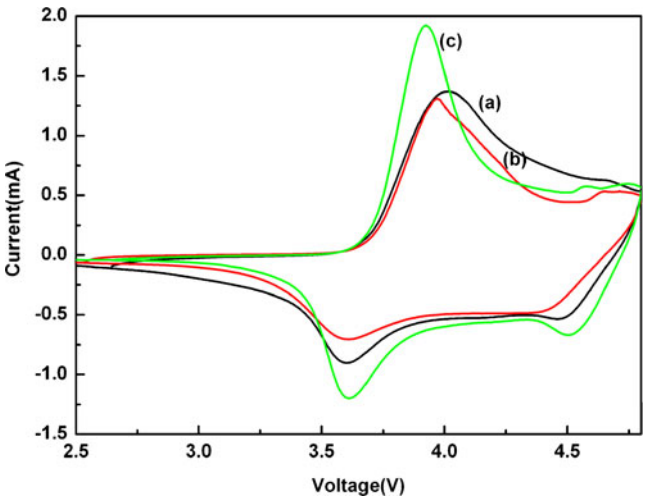

Fig. 13 Cyclic voltammograms for the prepared $LiNi_{1/3}Co_{1/3}Mn_{1/3}O_2$ **a** sample AH, **b** sample AS, and **c** sample AB at scan rate of 0.1 mV s^{-1} between 2.5 and 4.8 V

(2 C), and 135.9 mA g^{-1} (5 C), respectively. Therefore, NH_4HCO_3 is a good choice of complexant for the preparation of $[Ni_{1/3}Co_{1/3}Mn_{1/3}]CO_3$ as the precursor of $LiNi_{1/3}Co_{1/3}Mn_{1/3}O_2$ cathode material with excellent performance.

Acknowledgments This work is funded by the National Natural Science Foundation of China under project no. 20871101, Scientific Research Fund of Hunan Provincial Education Department no. 09C947, Key Project of Science and Technology Department of Hunan Province Government under project no. 2009WK2007, and Colleges and Universities in Hunan Province plans to graduate research and innovation under project no. CX2009B133.

References

1. Ohzuku T, Makimura Y (2001) Chem Lett 30:642–643
2. MacNeil DD, Lu Z, Dahn JR (2002) J Electrochem Soc 149: A1332–A1336
3. Cheralathan KK, Kang NY, Park HS, Lee YJ, Choi WC, Ko YS, Park YK (2010) J Power Sources 195:1486–1494
4. Park SH, Shin HS, Myung ST, Yoon CS, Amine K, Sun YK (2005) Chem Mater 17:6–8
5. Sun YK, Myung ST, Park BC, Prakash J, Belharouak I, Amine K (2009) Nat Mater 8:320–324
6. Shaju KM, Bruce PG (2006) Adv Mater 18:2330–2334
7. Li DC, Muta T, Zhang LQ, Yoshio M, Noguchi H (2004) J Power Sources 132:150–155
8. Kim JM, Chung HT (2004) Electrochim Acta 49:937–944
9. Shizuka K, Kobayashi T, Okahara K, Okamoto K, Kanzaki S, Kanno R (2005) J Power Sources 146:589–593
10. Luo XF, Wang XY, Liao L, Gamboa S, Sebastian PJ (2006) J Power Sources 158:654–658
11. Shaju KM, Subba Rao GV, Chowdari BVR (2002) Electrochim Acta 48:145–151
12. Zhang XY, Jiang WJ, Mauger A, Lu Q, Gendrond F, Julien CM (2010) J Power Sources 195:1292–1301
13. Zhang S (2007) Electrochim Acta 52:7337–7342
14. Deng C, Liu L, Zhou W, Sun K, Sun D (2008) Electrochim Acta 53:2441–2447
15. Lee M-H, Kanga Y-J, Myung S-T, Sun Y-K (2004) Electrochim Acta 50:939–948
16. Lavela P, Sanchez L, Tirado JL, Bach S, Pereira-Ramos JP (1999) J Power Sources 84:75–79
17. Yoncheva M, Stoyanova R, Zhecheva E, Alcántara R, Tirado JL (2009) J Alloys Compd 475:96–101
18. Park SH, Kang SH, Belharouak I, Sun YK, Amine K (2008) J Power Sources 177:177–183
19. Ren HB, Huang YH, Wang YH, Li ZJ, Cai P, Peng ZH, Zhou YH (2009) Mater Chem Phys 117:41–45
20. Zhang S, Deng C, Fu BL, Yang SY, Ma L (2010) Powder Technol 198:373–380
21. Zhang S, Deng C, Yang SY, Niu H (2009) J Alloys Compd 484:519–523
22. Cho TH, Park SM, Yoshio M, Hirai T, Hideshima Y (2005) J Power Sources 142:306–312
23. He P, Wang HR, Qi L, Osaka T (2006) J Power Sources 160:627–632
24. Alexander LE (1969) X-ray diffraction methods in polymer science. Wiley, New York
25. Cho TH, Park SM, Yoshio M (2004) Chem Lett 33:704–705
26. Park SM, Cho TH, Yoshio M (2004) Chem Lett 33:748–749
27. Park KS, Cho MH, Jin SJ, Nahm KS (2004) Electrochem Solid-State Lett 7:A239–A241
28. Rougier A, Gravereau P, Delmas C (1996) J Electrochem Soc 143:1168–1175
29. Shin HS, Park SH, Bae YC, Sun YK (2005) Solid State Ionics 176:2577–2581
30. Reimers JN, Rossen E, Jones CD, Dahn JR (1993) Solid State Ionics 61:335–344
31. Ohzuku T, Ueda A, Nagayama M (1993) J Electrochem Soc 140:1862–1869
32. Wang ZX, Sun YC, Chen LQ, Huang XJ (2004) J Electrochem Soc 151:A914–A921
33. Paulsen JM, Thomas CL, Dahn JR (2000) J Electrochem Soc 147:861–868
34. Ohzuku T, Ueda A, Nagayama M, Iwakoshi Y, Komori H (1993) Electrochim Acta 38:1159–1167
35. Madhavi S, Subba Rao GV, Chowdari BVR, Li SFY (2001) J Electrochem Soc 148:A1279–A1286
36. Armstrong AR, Robertson AD, Gitzendanner R, Bruce PG (1999) J Solid State Chem 145:549–556
37. Kajiyama A, Takada K, Inada T, Kouguchi M, Kondo S, Watanabe M (2001) J Electrochem Soc 148:A981–A983